Dual Optimization Method of RF and Quasi-Static Field Simulations for Reduction of Eddy Currents Generated on 7T RF Coil Shielding

Yujuan Zhao[1], **Tiejun Zhao**[2], **Shailesh B. Raval**[1], **Narayanan Krishnamurthy**[1], **Hai Zheng**[1], **Chad T. Harris**[3], **William B. Handler**[3], **Blaine A. Chronik**[3], and **Tamer S. Ibrahim**[1,4]

[1]Department of Bioengineering, University of Pittsburgh, Pittsburgh, PA, USA

[2]Siemens Medical Solutions, Pittsburgh, PA, USA

[3]Department of Physics and Astronomy, University of Western Ontario, London, Ontario, Canada

[4]Department of Radiology, University of Pittsburgh, Pittsburgh, PA, USA

Abstract

Purpose—To optimize the design of radiofrequency (RF) shielding of transmit coils at 7T and reduce eddy currents generated on the RF shielding when imaging with rapid gradient waveforms.

Methods—One set of a four-element, 2×2 Tic-Tac-Toe (TTT) head coil structure is selected and constructed to study eddy currents on the RF coil shielding. The generated eddy currents are quantitatively studied in the time and frequency domains. The RF characteristics are studied using the finite-difference time-domain (FDTD) method. Five different kinds of RF shielding were tested on a 7T MRI scanner with phantoms and in-vivo human subjects.

Results—The eddy current simulation method is verified by the measurement results. Eddy currents induced by solid/intact and simple-structured slotted RF shielding can significantly distort the gradient fields. EPI images, B_1^+ maps and S matrix measurements verified that the proposed slot pattern can suppress the eddy currents while maintaining the RF characteristics of the transmit coil.

Conclusion—The presented dual-optimization method could be used to design the RF shielding and reduce the gradient field-induced eddy currents while maintaining the RF characteristics of the transmit coil.

Index

RF shielding; Eddy current simulation; Gradient coil model; Full wave RF simulation; 7T MRI; EPI

[†]**Address correspondence to:** Tamer S. Ibrahim, PhD, Associate Professor, Departments of Bioengineering and Radiology, and Magnetic Resonance Research Center, University of Pittsburgh, Pittsburgh, PA 15213, Ph: +1 412-383-6946; Fax: +1 412-647-9800, tibrahim@pitt.edu.

Introduction

Gradient magnetic fields are used for information encoding in MRI. The gradient magnetic fields ($10\ kHz$) (1) can induce eddy currents in conductive materials of the MRI system (superconducting magnets, RF and gradient coil shielding, etc.). The generated eddy currents decay exponentially with relatively long time constants, typically tens or hundreds of milliseconds (2), which in turn can generate a second, distorting, magnetic field in the region of interest (ROI). This second magnetic field can generate severe image artifacts (1); it can also offset the superconducting operation point of the main magnet and even cause quench problems (3). Previous works have proposed methods of calculation (3–8) and reduction of the eddy currents on the magnet cryostat (9); these include active gradient shielding (10) and pre-emphasis (11,12) methods. These system level eddy-current compensations are typically available on current clinical scanners. Besides these system level compensation methods, post-processing methods were also discussed for eddy current compensation (13–15). In general, the success of these gradient imperfection correction methods rely on the image contrast differences, the accuracy of the measurement of the actual k-space trajectories, and/or the model of the gradient field distortions.

Less discussed are quantitative studies and correction of the eddy currents due to the RF shielding of RF coils. The RF shielding can play a major factor in improving transmit efficiency as well as maintaining the distribution of the excitation field (16). Especially for ultrahigh field (7T) MRI, the RF shielding is oftentimes one essential component for the transmit coils (17–21). Proper design of the RF shielding is particularly critical for echo-planar imaging (EPI) and 7T MRI parallel transmission (PTX) applications, since many of the PTX trajectories use spiral or EPI type gradient waveforms and these gradient waveforms can change rapidly (22,23). The fast changing gradient waveforms induce intensive eddy currents that can considerably distort the image quality. Furthermore, different transmit RF coils (i.e. head/knee/breast) are used at 7T MRI system and the RF shielding varies with the different coil designs, rendering the system eddy current correction possibly insufficient. In addition, the spatially non-linear eddy current behavior in regions close to the RF coil copper shielding may also render the above-mentioned post-processing methods less reliable. As a result, eddy currents induced on RF coil copper shielding could be very problematic.

Several works have analyzed methods of adding axial and azimuthal slots to reduce eddy currents on the RF shielding for birdcage coils and TEM coils (24–29). Capacitors are sometimes added at specified locations between the slots to avoid high-frequency RF field radiations (27). Fingerprint-like patterns have also been utilized (27,30). Multiple thin copper layers were discussed and their performance could be somewhat transparent for the MR gradient fields and efficiently blocking high frequency electromagnetic emission (1). Slotted double sided copper shields could be used to reduce gradient fields induced eddy currents as the copper shielding will be close to opaque for the RF signal because of the large capacitance between the overlapped shields (29).

In this work, we propose a methodology that aims at minimizing eddy currents induced on RF-coil shielding. The induced gradient field distortion (due to eddy currents) is

quantitatively studied in the time and frequency domains. Successful MRI gradient fields' measurement validation is delivered to verify the simulation results. Eddy current characterization is also studied based on the eddy current response function. A comprehensive optimization method, guided by full wave electromagnetic simulation combined with the eddy current simulation, is developed to maintain the RF-coil's RF characteristics and simultaneously reduce low frequency magnetic field distortions due to eddy currents on the RF coil shielding. The methodology is successfully tested on a Siemens 7T human whole body scanner with 1) a four-element, 2×2 Tic-Tac-Toe transmit/receive (Tx/Rx) array design (31,32) with an oil phantom and two in-vivo human subjects and 2) an RF coil system composed of 5 sets of the 2×2 Tic Tac Toe transmit coil (total of 20 Tx elements) in conjunction with a 32-ch receive coil insert with 10 in-vivo human subjects.

Methods

The RF Coil

New RF coil designs are desirable (33) in order to approach optimal RF coil performance at ultrahigh fields (34–46). Various and extensive RF shielding designs, in terms of shape, thickness and dimensions, may be necessary in order to achieve the optimal RF coil performance (transmit field distribution and field intensity). The proposed methodology is intended to be effective with any RF coil design, shape and/or geometry whether it is azimuthally symmetric or follows 4-fold symmetry etc.; and/or possess distinctive RF current patterns on the coil shielding. In this work, one set of a four-element, 2×2 Tic-Tac-Toe (TTT) head coil structure is selected and constructed. The view from foot to head of the assembled head coil is shown in Figure 1(a1). This four-element module is placed on the top of the head and functions as a Tx/Rx coil. The five flat and square-shaped copper RF shielding panels are positioned around the 2×2 coil structure. These panels are designed in a fashion that copper shielding could be easily switched to different types (47). The schematics of these 5 panels of RF copper shielding (3D) are shown in Figure 1(a2). The side view of the copper shielding is shown in Figure 1(a3).

Gradient Field Induced Eddy Current Simulations

Approximate models of the Siemens (Erlangen, Germany) 7T MRI whole body gradient coils have been designed using the Stream Function Method (48) to match the size and region of gradient linearity of the coils in the system. The designed gradient coil wire loops are shown in Figure 1(b1–b3). The Siemens whole body gradient coil has the following characteristics: inner diameter is 683 mm; Gmax in x,y,z are 40/40/45 mT/m, respectively; maximum slew rate is 200 T/m/s; imaging FOV is 500×500×420 mm; linearity is 5%. Three gradient coils generate three essential gradient magnetic fields for image information encoding and they are: $B_z = G_x x$, $B_z = G_y y$, $B_z = G_z z$. Based the Maxwell Equations, there are concomitant fields with these three gradient fields. For X gradient coil, $B_x = G_x z$, $B_y = 0$; for Y gradient coil, $B_x = 0$, $B_y = G_y z$; for Z gradient coil, $B_x = -G_x x/2$, $B_y = -G_y y/2$. The Z component of the gradient fields is dominated at the center of the gradient coils, where the RF coil is placed (29).

Models of a 40- turn Z-gradient coil (radius of 341.5 mm and wire diameter of 6.7mm) and a 36-turn X-gradient coil (radius 341.5mm and wire diameter of 4.2 mm) were constructed in SolidWorks (Waltham, MA, USA). Z-gradient coil positions along the Z-axis are given in Table 1. The X, Z-gradient coils and the RF coil models are imported in the ANSYS Maxwell 14.0 (Canonsburg, PA, USA). The passing currents are set up to mimic the currents flow inside the gradient coil wires when applying different scan protocols. The eddy current distortions are calculated and studied in the time and frequency domains by the Maxwell Transient Solver and Eddy Current Solver respectively.

The simulated Z-gradient fields (time domain) are used to compare with the measurements. The eddy current characteristic is then studied based on a characterization method using the eddy current impulse response function (23,49). The eddy current-induced magnetic fields can be derived as the convolution of the negative time-derivative of the ideal gradient waveform and the eddy current response function $H(t,z)$ (49) (Eq. 1). In this work, $B_d(t,z)$ is the ideal gradient field and $B_E(t,z)$ is the eddy currents-induced gradient field. The eddy current impulse response function $H(t,z)$ is the sum of multiple exponential terms with constant time τ_n and variable amplitude parameters α_n (23,49) (Eq. 2).

$$B_E(t,z) = -\left(\frac{dB_d(t,z)}{dt} \otimes H(t,z) \right) \quad (1)$$

$$H(t,z) = u(t,z) \sum_{n=0}^{N-1} \alpha_n(z) e^{-t/\tau_n(z)} \quad (2)$$

where $u(t,z)$ is the unit step function and N is the number of the exponential terms.

The frequency domain results are used to compare the distortions from 1) X and Z-gradient coils, 2) different copper thicknesses, and 3) the top panel, since there is no top shielding for some RF coils (16–18,24). These gradient field simulation results are used as a guide for the study of the eddy current reduction.

Full Wave RF Field Simulations

Effective RF shielding should provide efficient decoupling between the RF coil and the gradient coil without degrading the RF coils' performance (29). In the other words, properly designed RF coil shielding should be transparent to low time varying MR gradient fields and accommodating/supporting for high frequency RF fields. Therefore, the goal of the study is to maintain the characteristics of 7T RF coils (B_1^+ field distribution, B_1^+ intensity, E field distribution, and E field intensity) while reducing the induced low frequency eddy currents. An in-house Finite-difference time-domain (FDTD) package with an accurate transmission-line feed model mechanism is implemented to model the RF performance of the TTT coil (50). The RF magnetic field inside this four-channel TTT transceiver coil is modeled. The Discrete Fourier Transform (DFT) method is applied in order to calculate the RF currents (densities and directions) on the coil shielding at 297 MHz (7T MRI). The RF currents on the coil shielding are examined for multiple types of RF excitations (varying phases and amplitudes) resembling RF/B_1^+ shimming on a PTX system.

RF Testing and 7T Experiments

The gradient field simulation is verified on the 7T Siemens whole body scanner using the gradient field raw data measured inside a spherical oil phantom (diameter = 165 mm). To measure the gradient fields, a pair of trapezoidal gradients is applied multiple times at different slice locations (23,47). The gradient amplitude is ±2.0 mT/m, gradient slew rate is 40.0 mT/m/ms and pulse duration is 2.5 ms. Slots of the shielding and multiple thin copper layers are tested. S matrix measurements, B_1^+ maps and EPI sequences with the phantom and in-vivo human subjects are performed to verify the effectiveness of the proposed dual optimization. For EPI acquisition, the image resolution is 64 by 64; bandwidth per pixel is 2442 Hz/Px; TE and TR are 20 ms and 2000 ms respectively.

Results

Eddy Current Simulation Verification and Z Gradient Field Behavior along the Magnet Axis

The simulated Z gradient field in the time domain is displayed in Figure 2(a2). The ideal gradient strength and gradient strength associated with the presence of the TTT coil structure were compared at different positions along the Z direction (positive direction is defined towards the top panel of the RF coil). The isocenter was labeled as the center of the coil structure. The ideal gradient ramp up time is 50 μs. The results show that simulated Gz is deviating from the ideal Gz (0 to ~200 μs) due to eddy currents induced on the RF coil shielding. After ~200 μs, the simulated Gz becomes stabilized and equals to the ideal Gz. Figure 2(a1) shows the measured gradient waveform. The effective ramp up time of the measured gradient trajectories with the shielding is shown to be ~200 μs in agreement with the simulation results. Similar to the simulation results, the experimental results also demonstrate that eddy current distortion is non-linear and asymmetric along the Z direction.

To further study the eddy currents along the magnet axis, the simulated information was used to obtain the pulse response function $H(t,z)$ the by Eqs. 1 and 2. The results show that $H(t,z)$ has different characteristics at positive and negative positions due to the RF coil top panel. Figure 2(b1) demonstrates that $H(t,z)$ is not a linear with respect to Z. The eddy current effects are more prevalent in positive 60 mm position than the negative 60 mm position as shown in Figure 2(b2): $H(t,z)$ is (−80, −13, 0) at −60 mm and (133, 55, 15) at 60 mm, at 0 μs, 60 μs and 120 μs respectively.

Effects of Thickness of Copper Layers and the Top Panel

Thin copper shielding could be applied to improve the transparency to the gradient fields. The skin depth of copper at 297 MHz is about 4 μm and the 4 μm copper is also the thinnest copper we have found available in the market. We tested single 4 μm and double 4 μm (2×4 μm) copper shielding (Polyflon Company, Norwalk, CT, USA.) For the double layer copper shielding, the dielectric substrate between the two copper layers is 0.010" (0.25 mm) PTFE.

In order to compare the effects of 4 μm and a thicker (18 μm) copper shielding, simulation studies were performed. Figures 2(c1–c12) display the X, Z-gradient fields inside the RF coil at the Y=0 plane. When there was no RF shielding, the field was spatially linear along the X and Z directions for X and Z gradient coils respectively (Figures 2(c1) and 2(c7).)

When there were 18 μm and 4 μm copper shielding, the field was distorted (Figures 2(c2), 2(c4), 2(c8) and 2(c10).) In general, X-gradient fields induced less distortion than Z-gradient fields. Although the 4 μm copper sheets generated much less eddy current distortions than 18 μm copper, there were still observable residual distortions near the top panel (Figures 2(c3), 2(c5), 2(c9) and 2(c11).) Simulation studies (not shown) also demonstrate that the field distortion is more severe at higher gradient field frequencies.

The 4 μm intact (no slots) copper shielding panels are shown in Figure 3 (a1–a2). They are square shaped and the length of the copper panel is approximately 23 cm. The EPI images (Figures 3(b1)–3(b2)) were acquired to show the image distortions generated by the eddy currents when all 5 copper panels are present. In every subfigure, there are 11 slices shown at adjacent positions along the B_0 direction (one slice in one red frame box is used to point out the relative position within the EPI images.)

Effects of Simple-Structured Slots

Simple-structured slots along the axial direction was shown to be an effective way to reduce the eddy current effects (29). Simulation studies demonstrate that:

1. slots along the gradient field's changing direction are effective in reducing eddy current artifacts. As the X-gradient coil and Z-gradient coil generated fields are changing along the X direction and the Z direction, respectively, the slots should be cut along X direction and Z direction respectively;

2. three slots on each of the 4-μm shielding panels considerably suppress the eddy currents at 10 kHz. Since the distortion from the eddy currents is a function of the thickness of the copper sheets and the frequency of the gradient fields, more copper slots will be needed at higher frequencies and with thicker copper shielding: e.g., for 18 μm single copper, five slots can get similar suppression of the generated eddy currents; and

3. slots orthogonal to the gradient field changing direction don't reduce eddy currents.

The simple-structured slots have been physically applied to the double 4 μm (2×4 μm) copper shielding and 18 slots were etched on both sides of the copper shielding Figure 3(a3). The slots were staggered at both sides in order to minimize RF field leakage through the gap. EPI images (Figure 3(b3)) show the eddy current suppression was achieved, while the signal to noise (SNR) is very low. S parameter was measured to study the coil performance for different copper shielding. Figures 3(c1–c2) represent the network analyzer measured and FDTD simulated reflection coefficients with the intact 4 μm copper shielding. All reflection coefficients (Sxx) of the four ports are less than −18 dB. Figure 3(c3) shows the reflection coefficients (simulated and measured) for the simple-structured slot panel. For the pair of coil elements along the direction of the slots, the reflection coefficient (S11) is significantly different from the pair of coil elements orthogonal to the slots (S22); yet all the coil elements are detuned. The results also show that the coupling of the coil elements along the direction of the slots is −4.97 dB while the other two elements coupled by −14.7 dB. The coil cannot be re-tuned with this arrangement.

Dual Optimization Approach

Figures 3(d1) and 3(e1) display the FDTD calculated RF current distribution associated with four different excitation modes. Figure 3(e1) displays overlaid RF current vectors for the four excitation modes. The results show that with different transmit excitation modes (as used in PTX applications), the current densities and distribution patterns can be substantially different. Especially in the center areas, the current directions are substantially spatially changing with different types of excitations (as shown in the zoomed subfigures.) While the current distributions and current vectors are different for various excitation mechanisms, several locations on the shielding panels sustain minimal RF current densities (this was observed throughout all the modes and useful RF shimming patterns excited with the 2×2 TTT coil.) Based on these findings, the double 4 μm (2×4 μm) copper shielding were etched into different slotting patterns which are shown in Figure 3 (a4). The inner side of the top panel is slotted at regions where there is relatively lower RF current density in order to maintain the main RF current pathways. The external copper layers (facing the magnet) cuts (designed exclusively based on eddy current simulations) are used to reduce the eddy currents).

The low frequency eddy current simulations were then performed and verified that the induced eddy current was significantly reduced with the proposed slots which are shown for X-gradient coil in Figure 2(c6) and Z-gradient coil in 2(c12). For the RF characteristics, Figure 3(c4) demonstrates that the proposed slot patterns maintain the tuning and the matching of the RF coil as when intact shielding is utilized. From the EPI images in Figure 3(b4), the proposed slots in the double 4 μm (2×4 μm) copper shielding are highly effective in almost negating all of the eddy current artifacts and maintaining the RF characteristics of the RF coil. The SNR and B_1^+ maps have been measured to compare RF signal intensity/ distribution changes with different shielding thickness and patterns applied. When compared to the intact double-layered shielding, over all the slices, the SNR and B_1^+ distribution changes per slice are less than 5% when the proposed slot pattern is applied.

Figures 3(d3) and 3(e3) show the RF current distribution and current vectors were comparable with that of the intact copper, while Figures 3(d2) and 3(e2) show the RF currents were significantly distorted by the simple slots.

In-Vivo Demonstration

Healthy human subject studies were conducted, with signed consent forms approved by the Institutional Review Board at the University of Pittsburgh. In-vivo images acquired using the 4 element Tx/Rx coil with the proposed double 4 μm layer copper shielding and the 18 μm copper shielding are shown in Figures 4(a) and 4(b) respectively. In every image, there are 22 slices covering the whole human head. Because of eddy current artifacts, brain images are overlapped in almost every slice in the 18 μm copper case Figure 4(b). In the proposed slotted copper case Figure 4(a), images are intact (except near the absolute top of the human head.)

Discussion

Thin copper shielding was shown to improve the transparency to the gradient fields (1). However, the EPI images were distorted by artifacts even when the thin copper is used (4 μm single-layer which is the skin-depth of copper at 297 MHz and double-layered thin copper shielding) as demonstrated by Figures 2 and 3(b1–b2). Furthermore, simple-structured slots in double layer copper shielding have also been used to reduce gradient field-induced eddy currents (24,29). However as shown for our results, the suppressed eddy current distortion was achieved while significantly altering the coil RF characteristics (tuning, matching, coupling and RF current distribution/intensity on the coil shielding, and consequentially changes in the B1+ distribution/intensity etc..)

When using simple slots in the double layer copper shielding, the shield can be considered as a number of capacitors in parallel. The capacitance is proportional to the overlapping copper area and the thickness of the dielectric substrate in between. With the thin dielectric substrate in this study, the double layer copper with staggered slots should represent a thicker continuous conductor at 297MHz. Therefore the low SNR (Figure 3(b3)) was not necessarily caused by RF radiation/leaking. The changes in the coil's S parameters (Figure 3(c3)) and RF current distributions/densities on the coil's shielding (Figures 3(d2) and 3(e2)) show that the simple slots altered the RF coil's characteristics resulting in SNR reduction.

Figure 5 shows the ghosting quantitative comparisons between five different copper shielding patterns proposed and tested in this study, using the data measured from the phantom EPI images. The curves are the ratio between the background intensity (including noise and ghosting) and the image signal intensity. It shows less ghosting induced by the 4μm single and double-sided copper shielding when compared to the 18μm solid copper, through most of the slices. There is minimal eddy current induced ghosting in images associated with the simple-structured slots (Figure 3(b3)). However, the RF coil performance was deteriorated and Figure 4 shows that the background to signal intensity ratio is almost 50%. As a result and for the presented configuration, the use of thin copper layers and/or simple-structured slots for RF shielding was not effective in reducing the gradient field-induced low frequency eddy currents while maintaining the RF characteristics for this RF coil.

Some eddy current artifacts are present towards the top of the brain, shown in Figure 4(a) and Figure 5 curve for the proposed cut case. This could be caused by the copper on the Tx/Rx coil elements (copper struts) and on the small side panels which are covered by 18 μm copper sheets in the original coil design. These copper sheets can also generate eddy currents. Hence, the 18 μm copper sheets on the copper struts have been replaced by the thinner (9 μm) copper layers. And in order to provide a better and more realistic brain imaging illustration, an RF coil system composed of 5 sets of the 2×2 Tic Tac Toe transmit coil (total of 20 Tx channels) in conjunction with 32-ch receive coil insert was used. The copper shielding of the large panels of this 20 element transmit coil is similar to the tested 4 element Tx/Rx coil. However this RF coil system contains 1) 16 additional transmit elements with their 4 sets of small side panels in order to provide better transmit and

2) receive coil insert in order to provide better SNR. The in-vivo EPI images are shown in Figure 6 (a) (the image resolution= 96 by 96; bandwidth per pixel = 1680 Hz/Px; TE and TR = 24 ms and 2000 ms, respectively.) In order to display the background artifacts clearly, the intensity of 5 EPI image slices (showing the top of the head) was scaled by 10 times in Figure 6(b). Figure 6 shows that the ratio between the background intensity (including noise and ghosting) and the image signal intensity is less than 10%. Figures 2, 3, 4, 5 and 6 demonstrate the effectiveness of the proposed slotting method in reducing eddy current artifacts. In our experiences, the eddy current artifacts of this modified proposed slotted coil are comparable to other commercial non-shielded 7T RF coils.

In summary, five different types of copper shielding were tested and discussed in this study: single 18 μm (half oz) copper sheet, single 4 μm (0.114 oz) copper sheet, double 4 μm (2×4 μm) copper sheet, double 4 μm (2×4 μm) copper with simple-structured slots and double 4 μm (2×4 μm) copper with a proposed (based on RF and quasi-static field simulations) slot pattern specific to the RF coil (Tic-Tac-Toe transmit array) used. The eddy current simulations were verified with experimental data.

The results demonstrate that eddy currents induced on RF coil copper shielding can significantly distort the linear gradient fields. Although thinner copper shielding generated less (yet still considerable) distortion, the distortions due to the top (cap) copper shielding were significant. Simple slots along gradient field changing direction are verified to be an effective way to reduce the eddy current effects. However, simple-structured slots significantly altered the coil's RF characteristics (tuning, matching, coupling and RF current distribution/density on the coil shielding and consequentially transmit field intensity and distribution). This is critical when RF shielding is an essential (not just for the purpose of reduction of radiation) part of the coil performance as in the case of many high field transmit arrays.

Normally the golden rule used to sustain the RF performance is maintaining the RF current paths. However the RF current distribution as well as current direction could be different for different excitations modes, especially when a PTX system is used. In this work, using the proposed dual optimization method that combines both RF and quasi-static field simulations, the shield areas where there is minimal RF current density were distinctively slotted to maintain the main RF current density pathways. EPI images, GRE images, B_1^+ maps and network analyzer measurements verified that the proposed (based on RF and quasi-static field simulations) slot pattern in the double 4 μm (2×4 μm) copper sheet can sufficiently suppress the eddy current artifacts while maintaining RF characteristics of the utilized RF transmit array. This integrated, RF and quasi-static, field simulation approach can be utilized in designing RF coil shielding.

Acknowledgement

References

1. Truhn D, Kiessling F, Schulz V. Optimized RF shielding techniques for simultaneous PET/MR. Med Phys. 2011; 38(7):3995–4000. [PubMed: 21858996]

2. Jehenson P, Westphal M, Schuff N. Analytical Method for the Compensation of Eddy-Current Effects Induced by Pulsed Magnetic-Field Gradients in Nmr Systems. J Magn Reson. 1990; 90(2): 264–278.

3. Trakic A, Wang H, Liu F, Lopez HS, Crozier S. Analysis of transient eddy currents in MRI using a cylindrical FDTD method. Ieee T Appl Supercon. 2006; 16(3):1924–1936.

4. Tang F, Lopez HS, Freschi F, Smith E, Li Y, Fuentes M, Liu F, Repetto M, Crozier S. Skin and proximity effects in the conductors of split gradient coils for a hybrid Linac-MRI scanner. J Magn Reson. 2014; 242C:86–94. [PubMed: 24607826]

5. Sanchez Lopez H, Freschi F, Trakic A, Smith E, Herbert J, Fuentes M, Wilson S, Liu L, Repetto M, Crozier S. Multilayer integral method for simulation of eddy currents in thin volumes of arbitrary geometry produced by MRI gradient coils. Magn Reson Med. 2014; 71(5):1912–1922. [PubMed: 23818162]

6. Harris CT, Haw DW, Handler WB, Chronik BA. Application and experimental validation of an integral method for simulation of gradient-induced eddy currents on conducting surfaces during magnetic resonance imaging. Phys Med Biol. 2013; 58(12):4367–4379. [PubMed: 23739174]

7. Sanchez Lopez H, Poole M, Crozier S. Eddy current simulation in thick cylinders of finite length induced by coils of arbitrary geometry. J Magn Reson. 2010; 207(2):251–261. [PubMed: 20888278]

8. Kroot JMB, van Eijndhoven SJL, van de Ven AAF. Eddy currents in a transverse MRI gradient coil. J Eng Math. 2008; 62(4):315–331.

9. Boesch C, Gruetter R, Martin E. Temporal and spatial analysis of fields generated by eddy currents in superconducting magnets: optimization of corrections and quantitative characterization of magnet/gradient systems. Magn Reson Med. 1991; 20(2):268–284. [PubMed: 1775052]

10. Chapman B, Mansfield P. Double Active Magnetic Screening of Coils in Nmr. J Phys D Appl Phys. 1986; 19(7):L129–L131.

11. Wysong RE, Madio DP, Lowe IJ. A Novel Eddy-Current Compensation Scheme for Pulsed Gradient Systems. Magnet Reson Med. 1994; 31(5):572–575.

12. Ganin A, King KF. General Electric Company (Waukesha, WI), assignee. Automatic measurement of gradient field distortion. United States. 2001

13. Duyn JH, Yang YH, Frank JA, van der Veen JW. Simple correction method for k-space trajectory deviations in MRI. J Magn Reson. 1998; 132(1):150–153. [PubMed: 9615415]

14. Mohammadi S, Moller HE, Kugel H, Muller DK, Deppe M. Correcting eddy current and motion effects by affine whole-brain registrations: evaluation of three-dimensional distortions and comparison with slicewise correction. Magn Reson Med. 2010; 64(4):1047–1056. [PubMed: 20574966]

15. Xu D, Maier JK, King KF, Collick BD, Wu G, Peters RD, Hinks RS. Prospective and retrospective high order eddy current mitigation for diffusion weighted echo planar imaging. Magn Reson Med. 2013; 70(5):1293–1305. [PubMed: 23325564]

16. Vaughan JT. An Improved Volume Coil for High Field MRI ISMRM. 1999:167.

17. Crozier S, Forbes LK, Roffmann WU, Luescher K, Doddrell DM. Currents and fields in shielded RF resonators for NMR/MRI. Meas Sci Technol. 1996; 7(7):1083–1086.

18. Adriany G, Van de Moortele PF, Wiesinger F, Moeller S, Strupp JP, Andersen P, Snyder C, Zhang X, Chen W, Pruessmann KP, Boesiger P, Vaughan T, Ugurbil K. Transmit and receive transmission line arrays for 7 Tesla parallel imaging. Magnet Reson Med. 2005; 53(2):434–445.

19. Novikov A. Advanced theory of driven birdcage resonator with losses for biomedical magnetic resonance imaging and spectroscopy. Magn Reson Imaging. 2011; 29(2):260–271. [PubMed: 20869184]

20. Tropp J. Image brightening in samples of high dielectric constant. J Magn Reson. 2004; 167(1):12–24. [PubMed: 14987593]

21. Wright SM. Full-wave analysis of planar radiofrequency coils and coil arrays with assumed current distribution. Concept Magnetic Res. 2002; 15(1):2–14.

22. Grissom W, Yip CY, Zhang Z, Stenger VA, Fessler JA, Noll DC. Spatial domain method for the design of RF pulses in multicoil parallel excitation. Magn Reson Med. 2006; 56(3):620–629. [PubMed: 16894579]

23. Zheng H, Zhao TJ, Qian YX, Ibrahim T, Boada F. Parallel transmission RF pulse design for eddy current correction at ultra high field. J Magn Reson. 2012; 221:139–146. [PubMed: 22789452]

24. Alecci M, Jezzard P. Characterization and reduction of gradient-induced eddy currents in the RF shield of a TEM resonator. Magnet Reson Med. 2002; 48(2):404–407.

25. Daniel J, Weyers QL. Shielding apparatus for magnetic resonance imaging. US. 2006

26. Vaughan JT, Adriany G, Garwood M, Yacoub E, Duong T, DelaBarre L, Andersen P, Ugurbil K. Detunable transverse electromagnetic (TEM) volume coil for high-field NMR. Magn Reson Med. 2002; 47(5):990–1000. [PubMed: 11979579]

27. Yao Z, Wu Y, Chmielewski T, Shvartsman S, Eagan T, Martens M, Brown R. Simulation guidelines for incisions patterns on RF shields. Concept Magn Reson B. 2012; 41B(2):37–49.

28. Jaskolski PLWWI, Eash, Matthew G. (Oconomowoc, WI); General Electric Company (Milwaukee, WI), assignee. Mutual inductance NMR RF coil matching device. United States. 1987

29. Jin, J-M. Electromagnetic analysis and design in magnetic resonance imaging. Boca Raton, Fla. etc.: CRC press; 1999. p. 174

30. Roemer PB, Edelstein WA. RF shield for RF coil contained within gradient coils of NMR imaging device United States. 1989

31. Ibrahim YZ, TS.; Zhao, T.; Krishnamurthy, N.; Wood, S.; Raval, S.; Kim, H. 20-to-8 Channel Tx Array with 32-channel Adjustable Receive-Only Insert for 7T Head Imaging. Salt Lake City, Utah: ISMRM; 2013. p. 4408

32. Ibrahim, TS.; Hue, Y-K.; Boada, FE.; Gilbert, R. Tic Tac Toe: Highly-Coupled, Load Insensitive Tx/Rx Array and a Quadrature Coil Without Lumped Capacitors. Toronto, Canada: 2008. p. 438

33. Lattanzi R, Sodickson DK. Ideal current patterns yielding optimal signal-to-noise ratio and specific absorption rate in magnetic resonance imaging: Computational methods and physical insights. Magnet Reson Med. 2012; 68(1):286–304.

34. Trakic A, Weber E, Li BK, Wang H, Liu F, Engstrom C, Crozier S. Electromechanical Design and Construction of a Rotating Radio-Frequency Coil System for Applications in Magnetic Resonance. Ieee T Bio-Med Eng. 2012; 59(4):1068–1075.

35. Freire MJ, Lopez MA, Meise F, Algarin JM, Jakob PM, Bock M, Marques R. A broadside-split-ring resonator-based coil for MRI at 7 T. IEEE Trans Med Imaging. 2013; 32(6):1081–1084. [PubMed: 23529081]

36. Raghuraman S, Mueller MF, Zbyn S, Baer P, Breuer FA, Friedrich KM, Trattnig S, Lanz T, Jakob PM. 12-channel receive array with a volume transmit coil for hand/wrist imaging at 7 T. J Magn Reson Imaging. 2013; 38(1):238–244. [PubMed: 23239405]

37. Brown R, Madelin G, Lattanzi R, Chang G, Regatte RR, Sodickson DK, Wiggins GC. Design of a nested eight-channel sodium and four-channel proton coil for 7T knee imaging. Magn Reson Med. 2013; 70(1):259–268. [PubMed: 22887123]

38. Pang Y, Xie Z, Xu D, Kelley DA, Nelson SJ, Vigneron DB, Zhang X. A dual-tuned quadrature volume coil with mixed lambda/2 and lambda/4 microstrip resonators for multinuclear MRSI at 7 T. Magn Reson Imaging. 2012; 30(2):290–298. [PubMed: 22055851]

39. Raaijmakers AJ, Ipek O, Klomp DW, Possanzini C, Harvey PR, Lagendijk JJ, van den Berg CA. Design of a radiative surface coil array element at 7 T: the single-side adapted dipole antenna. Magn Reson Med. 2011; 66(5):1488–1497. [PubMed: 21630342]

40. Metzger GJ, van de Moortele PF, Akgun C, Snyder CJ, Moeller S, Strupp J, Andersen P, Shrivastava D, Vaughan T, Ugurbil K, Adriany G. Performance of external and internal coil configurations for prostate investigations at 7 T. Magn Reson Med. 2010; 64(6):1625–1639. [PubMed: 20740657]

41. Gilbert KM, Curtis AT, Gati JS, Klassen LM, Villemaire LE, Menon RS. Transmit/receive radiofrequency coil with individually shielded elements. Magn Reson Med. 2010; 64(6):1640–1651. [PubMed: 20648678]

42. Brown R, Storey P, Geppert C, McGorty K, Leite AP, Babb J, Sodickson DK, Wiggins GC, Moy L. Breast MRI at 7 Tesla with a bilateral coil and T1-weighted acquisition with robust fat suppression: image evaluation and comparison with 3 Tesla. European radiology. 2013; 23(11): 2969–2978. [PubMed: 23896763]

43. Thalhammer C, Renz W, Winter L, Hezel F, Rieger J, Pfeiffer H, Graessl A, Seifert F, Hoffmann W, von Knobelsdorff-Brenkenhoff F, Tkachenko V, Schulz-Menger J, Kellman P, Niendorf T. Two-Dimensional Sixteen Channel Transmi eceive Coil Array for Cardiac MRI at 7.0 T: Design, Evaluation, d Application. J Magn Reson Imaging. 2012; 36(4):847–857. [PubMed: 22706727]

44. Wiggins, GC.; Mareyam, A.; Setsompop, K.; Alagappan, V.; Potthast, A.; Wald, LL. A Close-Fitting 7 Tesla 8 Channel Transmit/Receive Helmet Array with Dodecahedral Symmetry and B1 Variation Along Z. Toronto Canada: 2008. p. 148

45. Brunner DO, De Zanche N, Frohlich J, Paska J, Pruessmann KP. Travelling-wave nuclear magnetic resonance. Nature. 2009; 457(7232):994–U992. [PubMed: 19225521]

46. Aussenhofer SA, Webb AG. Design and evaluation of a detunable water-based quadrature HEM11 mode dielectric resonator as a new type of volume coil for high field MRI. Magn Reson Med. 2012; 68(4):1325–1331. [PubMed: 22887743]

47. Zhao, Y.; Stough, D.; Zheng, H.; Zhao, T.; Harris, CT.; Handler, WB.; Chronik, BA.; Boada, FE.; Ibrahim, TS. Maximizing RF efficiency and minimizing eddy current artifacts using RF and eddy current simulations. International Society of Magnetic Resonance in Medicine Melbourne; Australia: 2012. p. 536

48. Peeren GN. Stream function approach for determining optimal surface currents. J Comput Phys. 2003; 191(1):305–321.

49. Atkinson IC, Lu A, Thulborn KR. Characterization and correction of system delays and eddy currents for MR imaging with ultrashort echo-time and time-varying gradients. Magn Reson Med. 2009; 62(2):532–537. [PubMed: 19353662]

50. Ibrahim TS, Hue YK, Tang L. Understanding and manipulating the RF fields at high field MRI. NMR Biomed. 2009; 22(9):927–936. [PubMed: 19621335]
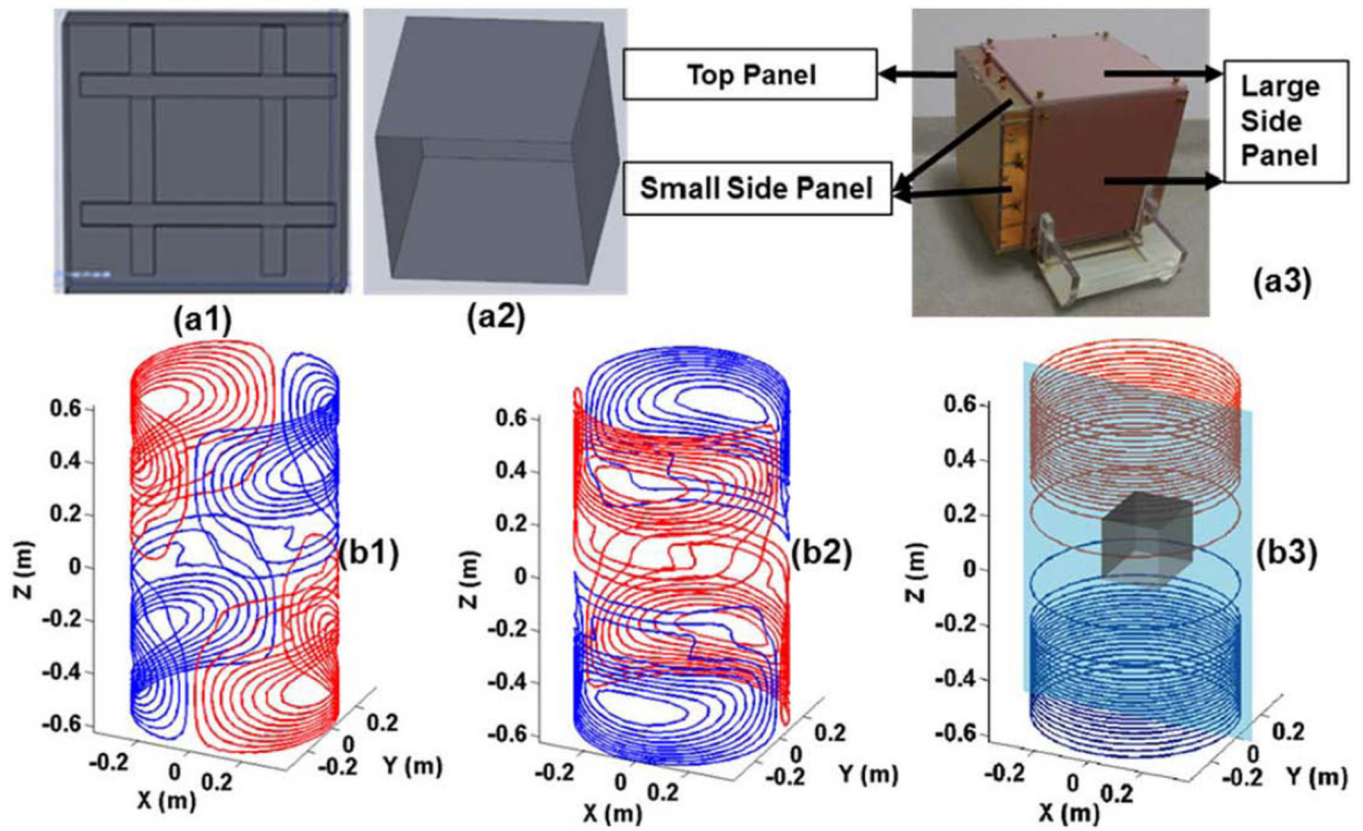
Figure 1.
Schematics of the (a1) Tic-Tac-Toe transmit/receive elements and (a2) RF shielding. (a3) Copper shielding components. Schematic diagrams of (b1) X gradient coil; (b2) Y gradient coil; (b3) Z gradient coil with the copper shielding to show the coil relative position. Red and blue colors indicate opposite current directions. The Y=0 plane is represented by the light blue color plane.
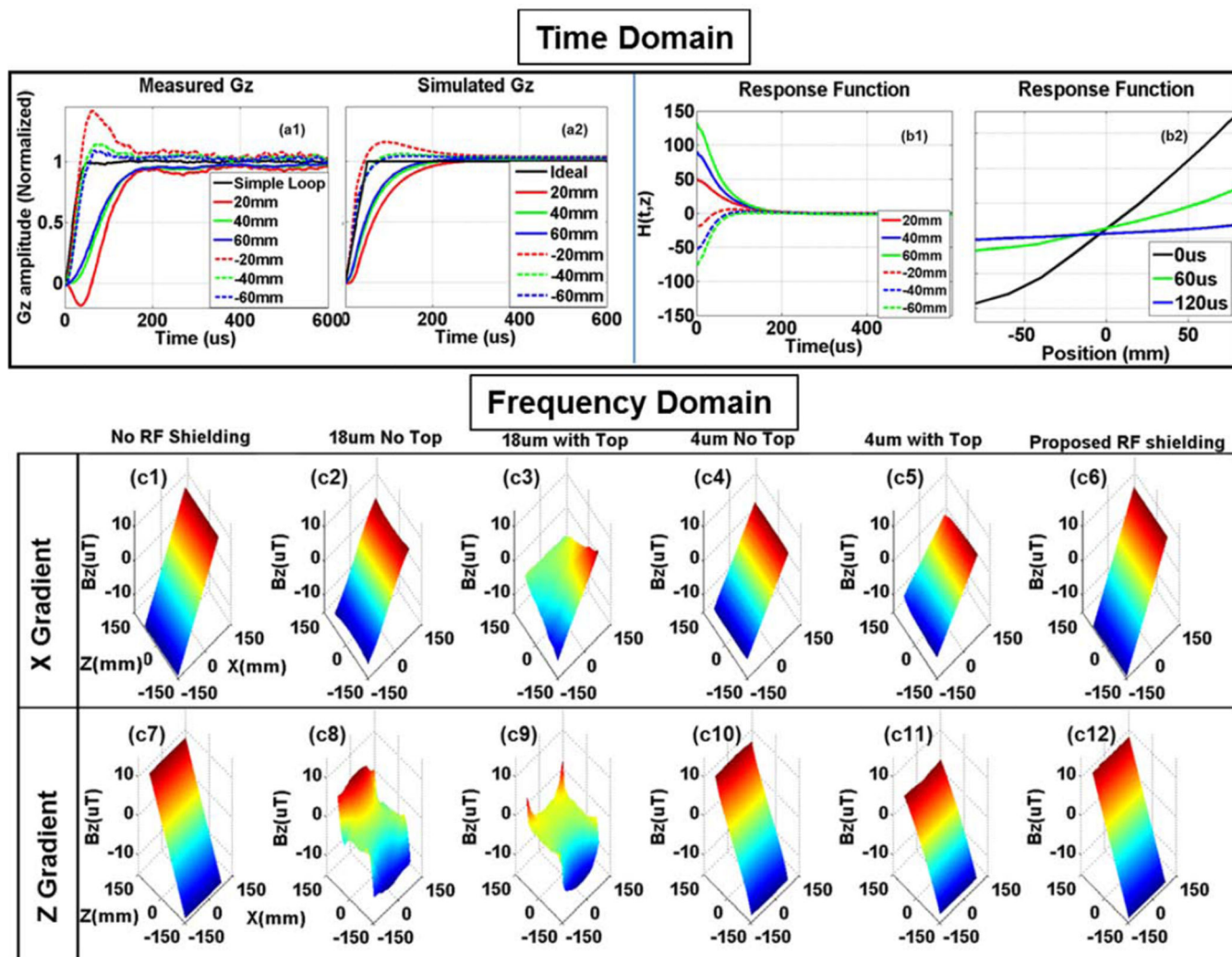
Figure 2.
Time domain: (a1) Normalized measured gradient field Gz at different positions along the Z direction. The curve for the "Simple Loop" was obtained using a simple RF loop-array coil without any RF shielding (used to represent the ideal gradient field in the measurements). (a2) Normalized simulated gradient field Gz at different positions along the Z direction. The "Ideal" Gz is calculated when the TTT coil structure is not present. (b1–b2) Eddy current pulse response function "H(t,z)" as a function of time and position (obtained by Eqs. 1 and 2.) Frequency domain: Six different cases have been used to study the top panel and copper thickness influence for X-gradient and Z-gradient fields. Positive "Z" positions are towards the top panel. Simulated gradient field distribution at the Y=0 plane are shown for 6 cases: 1) distribution with no RF copper shielding 2) distribution with intact 4 sides 18 μm and no top copper shielding 3) distribution with intact 5 sides 18 μm copper shielding 4) distribution with intact 4 sides 4 μm and no top copper shielding 5) distribution with intact 5 sides 4 μm copper shielding and 6) distribution with 5 sides 4 μm copper shielding that includes the proposed slots. (c1–c6) X-gradient field distributions at 10KHz and (c7–c12) Z-gradient field distributions at 10KHz.
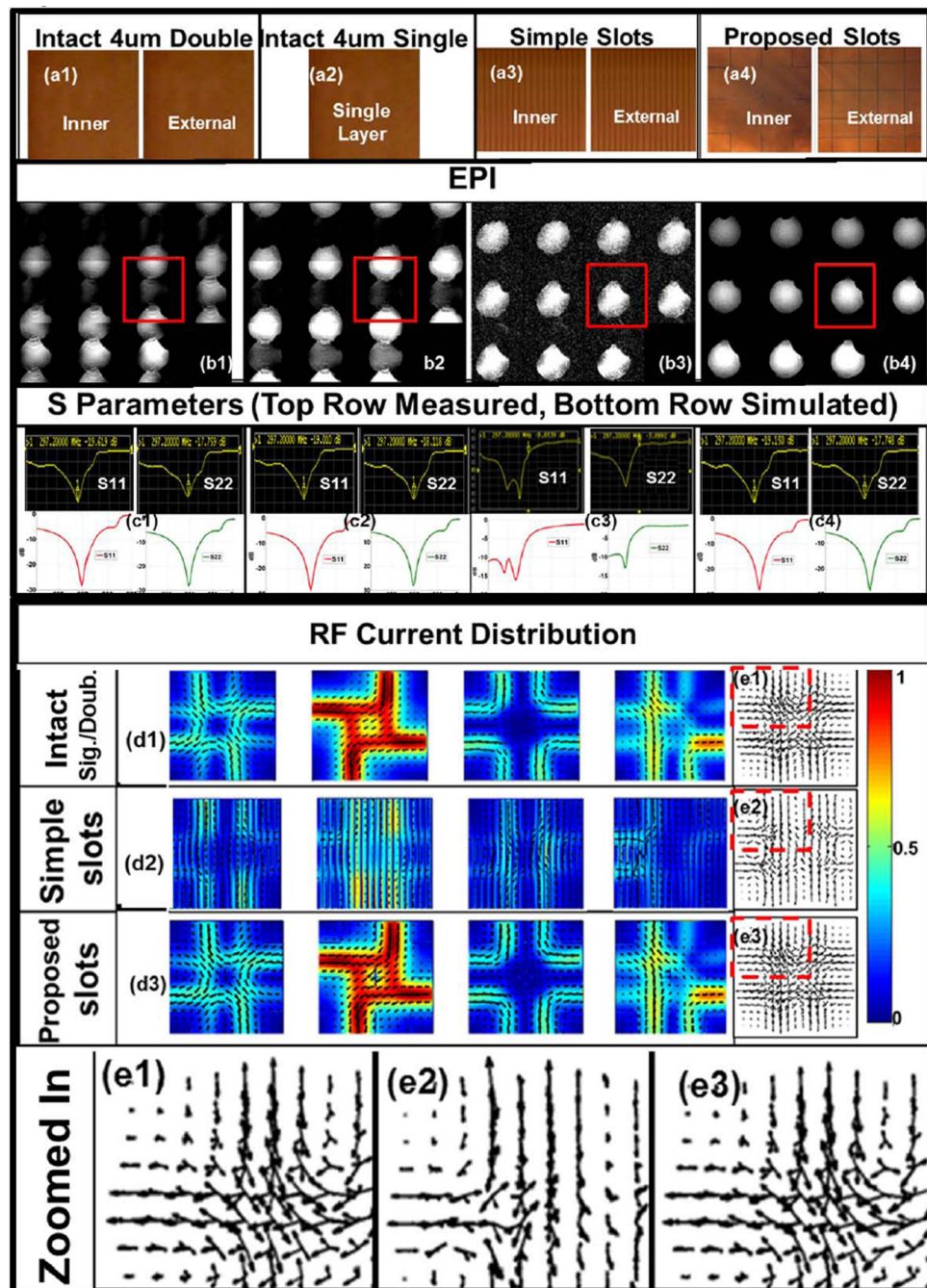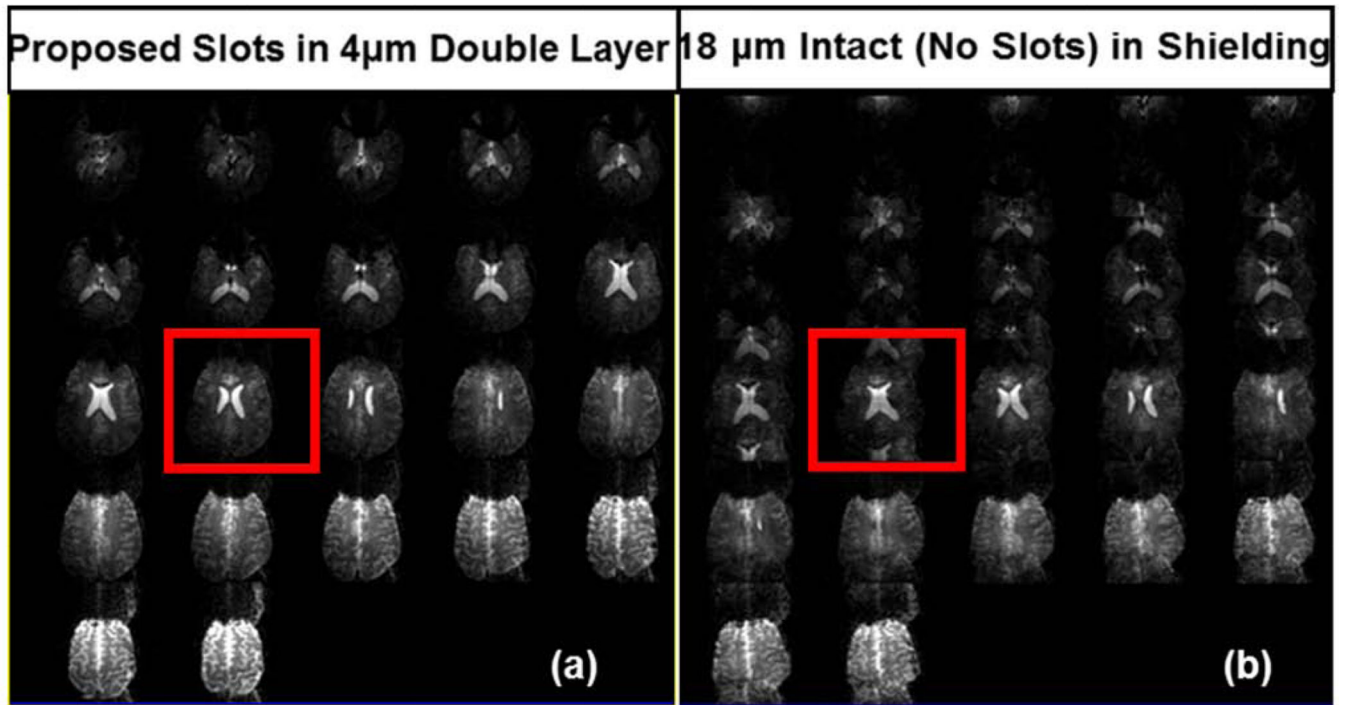
Figure 3.

Four different copper shielding comparisons. (a1) intact double 4 μm (2×4 μm) copper shielding, (a2) intact single 4 μm copper shielding, (a3) 18 longitudinal slots in the double 4 μm (2×4 μm) copper shielding and (a4) proposed copper slots in the double 4 μm (2×4 μm) copper shielding. The inner copper layer slots are based on the RF current distribution patterns and external copper layer slots are based on the eddy current simulations. (b1–b4) represents 11 slices of EPI images for the above-mentioned 4 copper shielding. (c1–c4) Reflection coefficients (measured and simulated using FDTD) for the transmit coil with the

above-mentioned 4 copper shielding. (d1–d3) RF currents on the copper shielding with four different excitation modes (uniform phase, quadrature, 180° phase shift between adjacent channels and one arbitrary set of 4 phases). The RF current distribution maps are presented at 297 MHz; plotted on the top of the density maps are the instantaneous current vectors. (e1–e3) Overlaid instantaneous RF current vectors of the four different excitation modes. The current vectors inside the red dashed box are zoomed in to show the vector patterns. (d1) and (e1) are for intact 4 μm single/double layer copper shielding, (d2) and (e2) are for the simple slots and (d3) and (e3) are for the proposed copper slots.
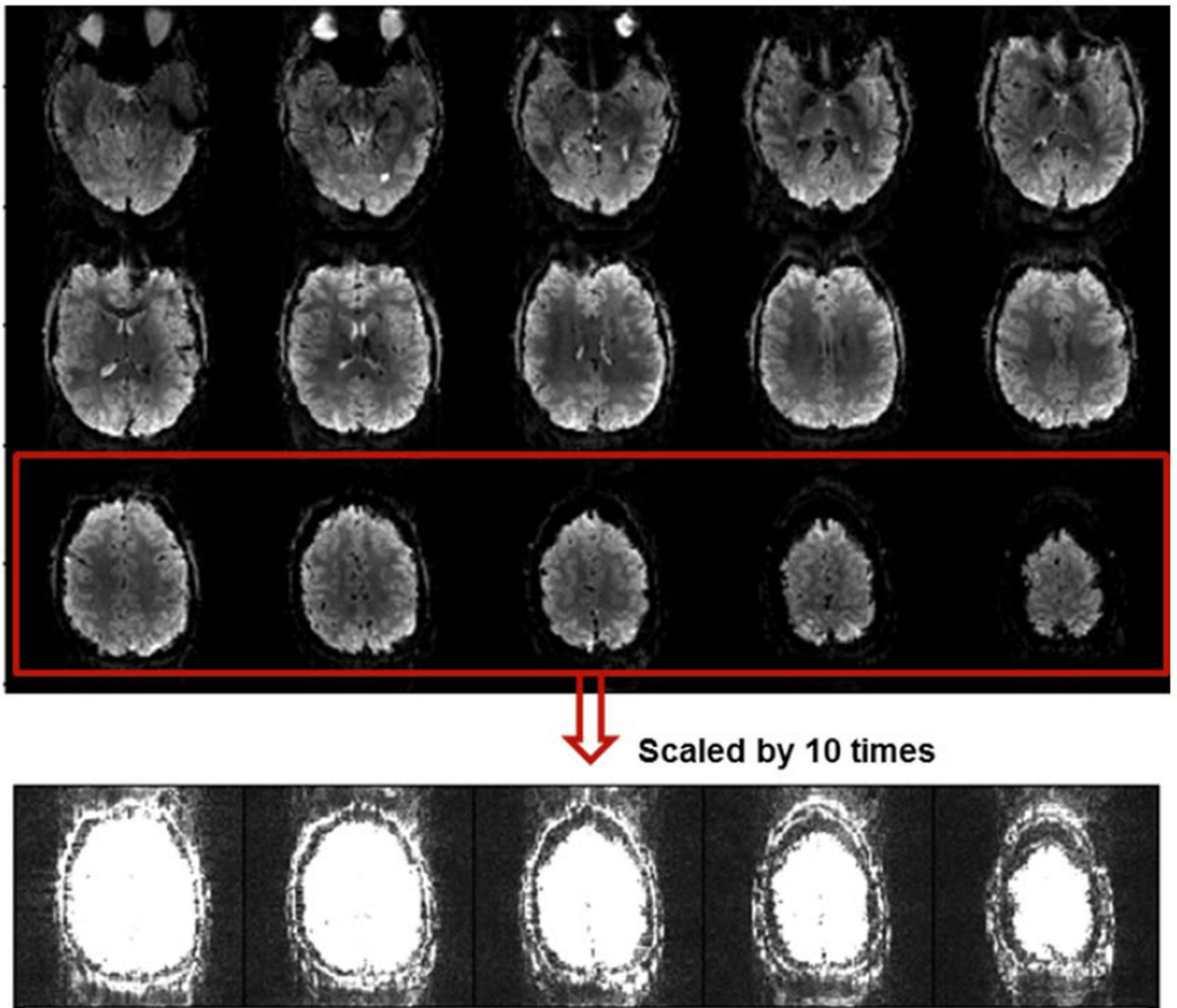
Figure 4.
In-vivo EPI images (22 slices to cover the whole brain) with (a) the proposed slots in double 4μm (2×4 μm) copper shielding and with (b) 18 μm intact/no-slots copper shielding.
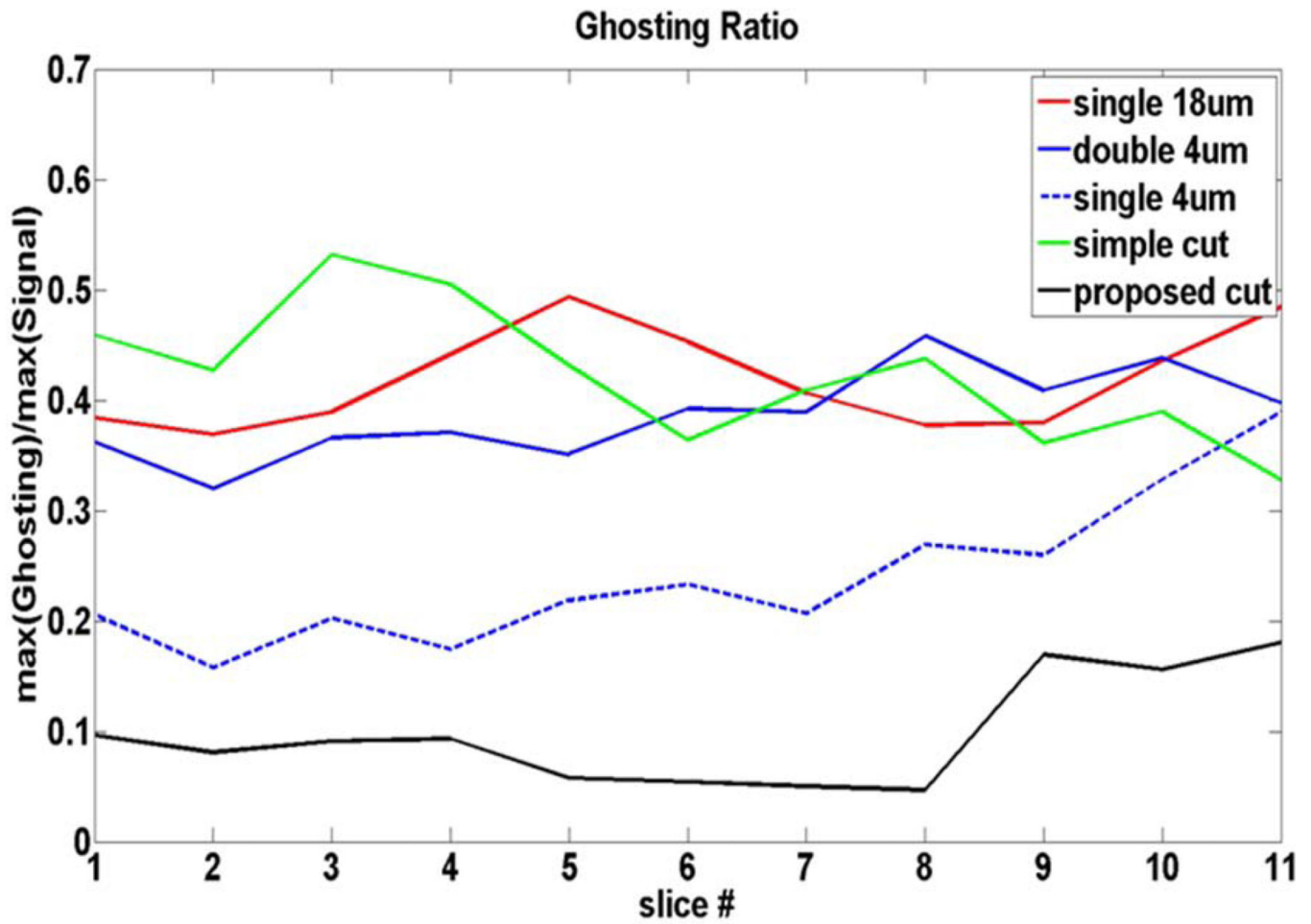
Figure 5.
Ghosting ratio comparisons (measured with EPI scans) between 5 tested/discussed copper shielding methods. The curves represent the ratio between maximum of the background intensity and the image signal intensity. Amongst the different shielding, the proposed shielding shows minimum ghosting.

Figure 6.
In-vivo EPI images with the modified slots in the double 4μm (2×4 μm) copper shielding using the 20-ch Tx coil with 32-ch Rx insert. The 5 top slices inside (a) are scaled by 10 times and shown in (b) to show the noise and eddy current ghosting distortion.

Table 1

Z-gradient coil arrangement

Coil positions along (±) z-axis (in mm)				
131	261	293	316	335
352	368	383	399	413
429	444	460	476	493
511	530	550	573	598